Received: 8 November 2024 | Revised: 8 January 2025 | Accepted: 23 February 2025

DOI: 10.1002/alz.70103

Alzheimer's & Dementia®
THE JOURNAL OF THE ALZHEIMER'S ASSOCIATION

RESEARCH ARTICLE

Structural changes in cerebral microvasculature induced by ferroptosis contribute to blood–brain barrier disruption in Alzheimer's disease: an autopsy study

Yuan Cao[1] | Mei-Ying Huang[1] | Chen-Hui Mao[1] | Xue Wang[2] | Yuan-Yuan Xu[2] | Xiao-Jing Qian[2] | Chao Ma[2] | Wen-Ying Qiu[2] | Yi-Cheng Zhu[1]

[1]Department of Neurology, State Key Laboratory of Complex Severe and Rare Diseases, Peking Union Medical College Hospital, Chinese Academy of Medical Sciences and Peking Union Medical College, Beijing, China

[2]Department of Human Anatomy, Histology and Embryology, Institute of Basic Medical Sciences, Neuroscience Center, Chinese Academy of Medical Sciences, School of Basic Medicine, Peking Union Medical College, Beijing, China

Correspondence
Yi-Cheng Zhu, Department of Neurology, State Key Laboratory of Complex Severe and Rare Diseases, Peking Union Medical College Hospital, Chinese Academy of Medical Sciences and Peking Union Medical College, Beijing 100730, China.
Email: zhuych910@163.com

Wen-Ying Qiu, Department of Human Anatomy, Histology and Embryology, Institute of Basic Medical Sciences, Neuroscience Center, Chinese Academy of Medical Sciences, School of Basic Medicine, Peking Union Medical College, Beijing 100730, China.
Email: qiuwy73@126.com

Funding information
STI2030-Major Project Task 5, Grant/Award Numbers: #2021ZD0201100, #2021ZD0201105; National Natural Science Foundation of China, Grant/Award Numbers: 81971138, 82301501; Chinese Academy of Medical Sciences Innovation Fund for Medical Sciences, Grant/Award Number: CIFMS 2021-I2M-1-025; Strategic Priority Research Program "Biological basis of aging and therapeutic strategies" of the Chinese Academy of Sciences, Grant/Award Number: XDB39040300

Abstract

INTRODUCTION: Cerebrovascular lesions are associated with cognitive impairment. However, the impact of AD neuropathological changes (ADNC) on cerebral microvasculature is not completely understood.

METHODS: Twelve decedents with ADNC and 15 matched controls were selected from the Brain Bank. The changes in the median tunica and basement membrane-related extracellular matrix (ECM) contents of the microvasculature were quantified and compared. Additionally, we explored the related mechanisms of agrin in pericytes.

RESULTS: Venular collagenosis was significantly more severe in AD patients ($p < 0.001$), and ECM remolding was significantly correlated with ADNC. In the AD group, blood–brain barrier (BBB) disruption and decreased pericytes were observed. Finally, we confirmed that agrin induced ferroptosis in pericytes and BBB disruption in vitro.

DISCUSSION: Our data indicate that venular collagenosis and significant ECM remolding are important contributors to ADNC. The mechanism by which agrin's role in disrupting the BBB by inducing ferroptosis presents a potential new target.

KEYWORDS
Alzheimer's disease neuropathological changes, arteriolosclerosis, cerebral microvasculature, extracellular matrix, pericyte ferroptosis, venular collagenosis

Highlights

- Changes in the median tunica and basement membrane-related ECM contents of the microvasculature were quantified in human brains.
- Venular collagenosis was significantly more severe in AD patients.

- In the AD group, BBB disruption and ECM remodeling were important contributors to AD neuropathological changes.
- Agrin disrupted the BBB by inducing ferroptosis in pericytes, which presents a potential new target.

1 | BACKGROUND

Alzheimer's disease (AD) neuropathological change (ADNC) is defined by the histological criteria of amyloid beta (Aβ) and tau deposition throughout brain regions,[1] which are common findings in aging brains.[2] According to *post mortem* studies, cerebrovascular lesions are found in as much as 80% of individuals with a clinical diagnosis of AD.[3,4] One proposed hypothesis is that microvasculature pathology enhances Aβ generation and reduces the elimination of abnormal protein deposits, thereby precipitating or hastening ADNC.[5,6]

Microvascular changes include arteriolosclerosis and venular collagenosis, both of which involve collagen deposits in medium. Arteriolosclerosis is widely regarded as an underlying contributor to ADNC based on both epidemiological and clinicopathological data [4]; however, venous collagenosis is an emerging finding in aging brains.[7] A preclinical histopathological study suggested an association between venous collagenosis and Aβ deposition[8]; nonetheless, evidence derived from human studies is limited. Considering that no study has compared the damage to arterioles and venules in correlation with ADNC, the type of small vessel that was the most important contributor remained unclear; this knowledge is important for understanding the mechanism by which microvascular factors contribute to the occurrence of ADNC since physiological functions differ significantly between arterioles and venules.[9–11]

Emerging evidence also suggests that the extracellular matrix (ECM) in the brain may play a role in the pathogenesis of AD.[12] The basement membrane (BM) is composed of uniform ECM at the abluminal surface of vascular endothelial cells, including collagen IV (Col IV), laminin, fibronectin, and heparan sulfate proteoglycans (HSPG) such as perlecan and agrin.[13] BM-related ECM not only provides a dynamic interface for cell communication but also contributes to the integrity of the BBB, which may correlate with ADNC progression.[14] However, previous studies on BM-related ECM changes in AD neuropathology have yielded variable results in human and animal models.[15–18] Additionally, these changes, including thickening of vascular walls and altered ECM protein levels, can also be detected in normal aging without the ADNC process.[19] Consequently, the comparison of BM-related ECM changes between patients with AD and normal-aging individuals has clinical significance.

Agrin, a specific ECM protein within the BM, has been implicated in BBB disruption.[20] Recent findings suggest that ferroptosis (an iron-dependent form of cell death) in pericytes could weaken the BBB and potentially facilitate ADNC progression.[21] However, the detailed mechanisms of agrin-induced ferroptosis in pericytes and its impact on the BBB in AD remain to be fully elucidated.

In this study, we aimed to investigate the association between microvascular lesions (in the media tunica and ECM contents) and ADNC (in both AD brains and age- and sex-matched normal brains). We evaluated the proportions of arteriolosclerosis, venular collagenosis, and levels of ECM components, including Col IV, laminin, fibronectin, perlecan, and agrin, in brain samples obtained from the white matter, cortex, putamen, and hippocampus of 27 donors. Additionally, we explored the potential mechanisms by which agrin influences pericyte ferroptosis and its role in BBB integrity.

2 | METHODS

2.1 | Antibodies and reagents

The following antibodies were used in this study: α-smooth muscular actin (αSMA, Cell Signaling Technology, 19245), monocarboxylate transporter 1 (MCT1, Proteintech, 20139-1-AP), Col IV (Abcam, ab6586), laminin (Abcam, ab11575), fibronectin (Abcam, ab2413), perlecan (Abcam, ab23418), agrin (Abcam, ab85174; Sigma-Aldrich, MAB5204), PDGFRβ (Proteintech, 13449-1-AP), Claudin-5 (Proteintech, 29767-1-AP), GPX4 (Abcam, ab125066), and FTH1 (Affinity Biosciences, DF6278). Recombinant human agrin protein (R&D Systems, 6624-AG), erastin (Proteintech, 571203-78-6), and Ferrostatin-1 (Fer-1, Proteintech, 347174-05-4) were also used.

2.2 | Brain sampling

Brain tissue was obtained at autopsy and stored within the National Human Brain Bank for Development and Function (http://anatomy.sbm.pumc.edu.cn/brainbank) in accordance with the Institutional Review Board of the Institute of Basic Medical Sciences of the Chinese Academy of Medical Sciences/Peking Union Medical College, Beijing, China (Approval No.: 009-2014, 031-2017, and 2022125). A more detailed description of the standardized protocol of the human brain bank in China was published elsewhere.[22] Written informed consent and basic demographic and medical information were obtained from the brain donors or their next of kin.

After removing the brain, it was weighed; the anteroposterior and left-to-right diameters were measured as brain volume. The right hemisphere was immersion-fixed in 10% buffered aqueous formaldehyde solution for 2 to 6 weeks and then subsequently dissected in coronal planes at approximately 1.0-cm intervals. A review of clinical records

TABLE 1 Basic characteristics of samples.

	AD group $n = 12$	Non-AD group $n = 15$	p value*
Age, mean ± SD (y)	80.0 ± 12.7	75.2 ± 15.2	0.389
Male, *n* (%)	6 (50.0)	7 (46.7)	0.863
Post mortem delay, median, IQR (h)	6.3 (4.0 to 11.0)	10.0 (5.0 to 21.0)	0.259
History			
None, *n* (%)	1 (8.3)	0 (0)	0.444
Tumor, *n* (%)	2 (16.7)	8 (53.3)	0.107
Dementia,[a] *n* (%)	7 (58.3)	0 (0)	<0.001
CHD, *n* (%)	0 (0)	1 (6.7)	1.000
Others,[b] *n* (%)	2 (16.7)	6 (40.0)	0.236
Brain weight, mean ± SD (g)	1148.5 ± 112.7	1138.4 ± 117.8	0.834
Brain volume, mean ± SD (cm^3)	1480.3 ± 603.7	1660.0 ± 342.4	0.415

Abbreviations: AD, Alzheimer's disease; CHD, coronary heart disease; IQR, interquartile range; SD, standard deviation.
[a]Clinically diagnosed dementia was recorded as patient history.
[b]Other history included chronic bronchitis, arrhythmia, pulmonary fibrosis, respiratory failure, and heart failure.
*p values were calculated using Student's t-test, Mann-Whitney U test, or Fisher's exact test.

RESEARCH IN CONTEXT

1. **Systematic review**: The authors reviewed the existing literature using primarily PubMed. Although many cerebrovascular lesions were associated with cognitive impairment, the implication of ADNC on cerebral microvasculature is not completely understood.
2. **Interpretation**: The findings show that venular injuries with severe collagenosis in the media tunica and significant basement membrane-related ECM remolding are important contributors to ADNC. Additionally, the study confirmed that agrin induced ferroptosis in pericytes and BBB disruption in vitro, which may accelerate ADNC progression.
3. **Future directions**: Future studies should pay more attention to the pathological changes in venules as a potential contributor to ADNC. Further studies are needed to delineate the precise molecular interactions between agrin, pericytes, and the ferroptotic pathway, as well as to explore the therapeutic potential of ferroptosis inhibitors in AD and related diseases.

after patients' death was undertaken (Q.W.Y.), and no evidence of stroke or brain tumor history until death was noted.

All brains underwent neuropathological assessment according to the National Institute on Aging-Alzheimer's Association criteria,[23] which included the assessment of Thal phases of Aβ deposition (A score),[24] Braak staging of neurofibrillary pathology (B score),[25] and Consortium to Establish a Registry for Alzheimer's disease scoring (C score).[26] Briefly, we performed immunohistochemistry for Aβ plaque detection using antibody 6F/3D (Novocastra, UK), B score (immunohistochemistry of neurofibrillary tangles) using phospho-tau antibody (Abcam, UK), and senile plaques (C score) by modified Bielschowsky stain. The protocol for the immunochemistry process of ADNC has been described elsewhere.[23] First, 12 patients with intermediate or high ADNC were selected and grouped into the AD group; then, 15 age- and sex-matched patients without ADNC were selected and grouped into the non-AD group. Finally, our study consisted of 27 human *post mortem* brains (mean age 77.33 ± 14.07 years; male: 13), and their clinicopathological profiles are shown in Table 1.

Tissue blocks were systematically collected from white matter regions of the cortex, putamen, and hippocampus and embedded in paraffin. Specifically, the white matter blocks included the frontal periventricular, occipital periventricular, and deep white matter in the parietal lobe, while the cortex blockers included the superior frontal cortex (Brodmann area 9) and occipital cortex (Brodmann areas 17 and 18). Therefore, seven regions were examined in this study. Paraffin-embedded serial sections from seven tissue blocks were cut to a thickness of 5 μm for further staining and evaluation.

2.3 | Image analysis

All image analyses were performed independently by two trained neurologists (C.Y. and H.M.Y.) and reviewed by a pathologist (Q.W.Y.), who was blinded to the neuropathological diagnosis, with an inter-observer correlation coefficient (ICC) of 0.91. Whole stained sections were scanned using an aperio digital pathology slide scanner (Leica Biosystems), and monochrome images were uploaded into the ImageJ software program (Media Cybernetics Inc., USA; version 6.3). Positive and negative controls were included in each batch.

2.3.1 | Evaluations of arteriolosclerosis and venular collagenosis

All sections from the white matter regions, cortex, putamen, and hippocampus were histologically stained with hematoxylin and eosin (H&E) and Masson's trichrome in adjacent slices. Immunohistochemistry was performed with antibodies against αSMA (Catalog No.: 19245, RRID: AB_2734735, rabbit monoclonal antibody, diluted 1:400; Cell Signaling Technology, Danvers, MA, USA) and MCT1 (Catalog No.: 20139-1-AP, RRID: AB_2878645, rabbit polyclonal antibody, diluted 1:800; Proteintech, Chicago, IL, USA) to distinguish between arterioles, capillaries, and venules (details on primary antibodies and antigen retrieval protocols for immunohistochemistry are presented in Table S1). Immunopositivity was detected using the VECTASTAIN ABC-HRP Kit (rabbit IgG, PK-4001; Vector Laboratories, Burlingame, CA, USA) with 3, 3′-diaminobenzidine (DAB) as a chromogen and hematoxylin as

the counterstain. All histologically and immunohistochemically stained sections were subsequently dehydrated using a series of alcohols and were cleared and mounted with neutral balsam mounting medium (ZLI-9555, ZSGB-BIO, Beijing, China).

To evaluate the severity of arteriolosclerosis and venular collagenosis, 2400 × 3800 μm single images were captured randomly in anti-αSMA and anti-MCT1 immunostained sections to differentiate between arterioles and venules, and the corresponding visual fields on the delineated images were subsequently captured in adjacent Masson's trichrome sections to assess the severity. For arteriolosclerosis evaluation, based on our previous report,[27] briefly, vessels from 10 to 200 μm in diameter that showed negative immunolabeling for MCT1 in endothelial cells and positive immunolabeling for αSMA in smooth muscle cells were considered arterioles. According to the vascular cognitive impairment neuropathology guidelines (VCING),[28,29] arteriolosclerosis was graded according to severity using histological semiquantitative scales ranging from 0 to 3 (0 = normal, 1 = mild changes, 2 = moderate changes, and 3 = severe changes). Arterioles scored 2 or 3 were assessed as arteriolosclerosis in our study, and the ratio of the number of sclerotic arterioles to total arterioles in the visual field was calculated. Similarly, venules were identified with intense labeling for MCT1 in the endothelium and a thin anti-αSMA staining pattern in the media tunica, and those with severe stenosis (the lumen occupying more than 50% of the vessel diameter) or occlusion by thick collagenous walls were assessed as venular collagenosis according to previous scores by Moody et al.[30] The ratio of the number of collagenized venules to the total number of venules in the visual field was calculated.

2.3.2 | Basement membrane-related ECM protein evaluation

ECM changes are evident in thickened microvessels, and the top 13 subjects with severe microvascular damage were selected and five randomly captured regions (1 × 1 mm) from each brain were evaluated. Finally, a subset of 65 regions (including 30 regions from AD cases and 35 regions from non-AD cases) from 13 brain tissues was fixed; immunohistochemistry was performed using antibodies against anti-Col IV (Catalog No.: ab6586, RRID: AB_305584, rabbit polyclonal antibody, diluted 1:800; Abcam, Cambridge, UK), anti-laminin (Catalog No.: ab11575, RRID: AB_298179, rabbit polyclonal antibody, diluted 1:400; Abcam, Cambridge, UK), anti-fibronectin (Catalog No.: ab2413, RRID: AB_2262874, rabbit polyclonal antibody, diluted 1:800; Abcam, Cambridge, UK), anti-perlecan (Catalog No.: ab23418, RRID: AB_2119099, mouse monoclonal antibody, 1:100; Abcam, Cambridge, UK), and anti-agrin (Catalog No.: ab85174, RRID: AB_1860988, rabbit polyclonal antibody, 1:100; Abcam, Cambridge, UK). For the immunohistochemical quantification of these ECM proteins, five 1 × 1 mm regions of interest (ROIs) were captured randomly, the inverted mean gray values of the area immunoreactive for DAB staining were measured using ImageJ software, and the mean values for the images were calculated for each region using the Mann–Whitney *U* test (raw immunohistochemistry data are provided in Tables S2 and S3).

2.4 | Cell culture

In this experiment, human microvascular pericytes (HVPCs, Catalog No.: HUM-iCell-n011) were obtained from iCell (http://www.icellbioscience.com) and cultured using a specialized primary human brain microvascular pericyte medium (Catalog No.: iCell-n011-002 h); the hCMEC/D3 cell line (Catalog No.: CL-0843) was purchased from Pricella (https://www.procell.com.cn) and cultured using a specialized hCMEC/D3 medium (Catalog No.: CM-0843).

To investigate the effects of agrin on the BBB, we developed an in vitro BBB model by co-culturing hCMEC/D3 cells with HVPCs in the transwell system (Figure S1). The detailed procedure is as follows:

Preparation of cells: hCMEC/D3 cells and pericytes were cultured in specialized cell culture medium under standard conditions (37°C, 5% CO_2). HVPCs were cultured and used between passages four and six.

Coculture setup: 100 μL of hCMEC/D3 cell suspension (5×10^5 cells) was seeded on the upper side of transwell inserts with a pore size of 0.4 μm (724121, NEST Biotechnology Co.), which allowed the interaction of soluble factors but prevented direct cell migration. A hundred microliters of HVPC suspension (5×10^5 cells) was seeded on the bottom of 12-well cell culture plates to mimic the perivascular environment. Inserts contained 1.5 mL medium in the basolateral compartment and 500 μL in the apical compartment.

Coculture conditions: The transwell system was maintained in specialized cell culture medium, which was replaced every other day until the establishment of an in vitro BBB model.

2.5 | Cell Counting Kit-8 assay of cell proliferation

This assay was conducted following the instructions of the Cell Counting Kit-8 (CCK-8; Dojindo, CK04). The steps were as follows. (1) First, 100 μL of HVPC suspension (1000 cells per well) was prepared in a 96-well plate, and the culture plate was placed in an incubator for 24 h (37°C, 5% CO_2). (2) After agrin (5, 10, or 50 μg/mL) treatment, the sample was added to the culture plate. (3) The culture plate was incubated in an incubator for 1, 2, 6, 12, and 24 h. (4) Then 10-μL CCK-8 solution was added to each well. (5) The culture plate was incubated in the incubator for 2 h. (6) The absorbance was measured at 450 nm with a microplate reader.

2.6 | Detection of ROS

The detection of ROS in cells using a ROS kit (Elabscience, E-BC-F005). The steps were as follows. (1) Seed cells in a cell culture dish with culture medium. (2) Discard supernatant and wash cells three times with a serum-free culture medium. (3) Add ROS probe working solution. (4) Incubate cells at 37°C, protected from light, for 60 min. (5) After

incubation, discard the working solution and wash the cells three times with serum-free cell culture medium to remove any unincorporated 2′,7′-dichlorodihydrofluorescein diacetate (DCF-HDA). (6) Immediately observe under a fluorescence microscope (Nikon) and evaluate using a multifunctional fluorescence microplate reader (excitation: 488 nm; emission: 610 nm, SpectraMax i3x Multi-Mode Microplate Reader, Molecular Devices). Fluorescence images were captured by selecting three ROIs per image using SlideViewer, and fluorescence intensity was calculated with four replicates for each condition. Statistical significance was determined using the Mann–Whitney *U* test.

2.7 | Annexin V-FITC/propidium iodide double-label staining to detect cell apoptosis

The steps were as follows. (1) The culture medium was discarded, and HVPCs were digested with 0.25% trypsin without EDTA at room temperature. After the cells were round and floating under the microscope, the digestion was immediately stopped with complete culture medium, and the cell suspension was transferred to a flow tube. (2) The sample was centrifuged at 1000 rpm, and the precipitate was left after 5 min. (3) The cells were washed twice with precooled PBS and resuspended at 1×10^6 cells/mL in 1 × buffer. (4) One hundred microliters of the resuspended cell solution were placed in a flow tube. (5) Then 5 μL of FITC Annexin V and 5 μL propidium iodide (PI) were added (E-CK-A211, Elabscience). (6) The sample was vortexed gently and incubated for 5 min at room temperature in the dark. (7) Then 400 μL of 1 × buffer was added to each tube for testing within 1 h. The cells were subsequently measured using an LSR II flow cytometer (BD Biosciences) and analyzed using FlowJo software.

The Annexin V-FITC/PI double labeling results were analyzed using FlowJo software, and the cells were categorized in the following four quadrants: lower left, live cells; lower right, early apoptosis; upper right, late apoptosis; and upper left, cell fragments. Data collection and analysis were performed.

2.8 | Immunofluorescence and confocal imaging

After the various treatments, cells seeded on coverslips were fixed with 4% ice-cold paraformaldehyde at room temperature for 15 min, followed by permeabilization with 0.1% Triton X-100/PBS. After incubation in blocking solution (5% BSA) at room temperature for 1 h, the cells were incubated with primary antibody at 4°C overnight. This step was followed by three washes in PBS. The cells were then incubated with goat anti-mouse IgG-Alexa Fluor Plus 488 (Thermo Fisher Scientific, A11029) or goat anti-rabbit IgG-Alexa Fluor Plus 647 (Thermo Fisher Scientific, A27040) for 1 h at room temperature. After the cells were washed with PBS three times, the coverslips were mounted onto glass slides using a fluorescent mounting medium. All confocal images were acquired and processed using a confocal microscope (Zeiss).

2.9 | Western blotting

Proteins from animal brains were homogenized, and cells were lysed with RIPA buffer (EpiZyme, PC101). The samples were loaded on gradient SDS–PAGE gels (EpiZyme, LK309), and the total protein concentration was determined by bicinchoninic acid assays (EpiZyme, ZJ102). The same amount of protein (30–50 mg) was loaded and run on SDS–PAGE gels, and the proteins were then transferred to nitrocellulose membranes (0.45 or 0.22 μm), which were blocked with 5% non-fat dry milk in 0.01 M PBS (pH 7.4) and 0.05% Tween-20 (PBST) at room temperature for 1 h. Subsequently, the membrane was incubated with primary antibodies directed against target proteins overnight at 4°C. The final dilutions for primary antibodies were as follows: after three quick washes in PBST, the membranes were incubated with secondary antibodies conjugated to HRP (Proteintech, SA00001-1, SA00001-2) diluted 1:2000 in PBST for 1 h. The final detection of immunoreactive bands was developed using an enhanced chemiluminescent Western blot system with exposure to a chemiluminescence imaging system. The immunoblotting signal intensity was measured using ImageJ software.

2.10 | Detection of intracellular Fe^{2+}

To detect intracellular Fe^{2+} levels, we used a FerroOrange fluorescent probe (DOJINDO, F374). The experiment was conducted as follows: (1) Cell preparation: Cells were seeded onto coverslips in a 24-well plate and allowed to adhere overnight at 37°C in a 5% CO_2 incubator. For quantification, cells were seeded in 96-well black-walled plates and incubated overnight under the same conditions. (2) FerroOrange staining: The culture medium was removed, and the cells were washed three times with serum-free culture medium. FerroOrange was diluted in Hank's balanced salt solution to a final concentration of 1 μmol L^{-1}, as recommended by the manufacturer. Cells were incubated with the FerroOrange staining solution at 37°C for 30 min in the dark. (3) Imaging: Observe the cells immediately under a fluorescence microscope after adding FerroOrange dye, without washing. The fluorescence signal of FerroOrange was captured using a fluorescence microscope (Nikon). Images were acquired under identical conditions across all experimental groups to ensure comparability. (4) Fluorescence intensity detection: The fluorescence intensity of each well was measured using a microplate reader (excitation: 543 nm; emission: 580 nm, SpectraMax i3x Multi-Mode Microplate Reader, Molecular Devices). The relative intracellular Fe^{2+} levels across different groups were analyzed using the Mann–Whitney *U* test ($n = 4$).

2.11 | Statistical analysis

SAS 9.4 (SAS Institute, Inc., Cary, NC, USA) was used for statistical evaluation. Variables were tested for normality using the Shapiro–Wilk test and visual inspection of variable histograms. Descriptive analyses were

conducted for continuous variables (using the mean and range) and categorical variables (percentage). To compare the ratio of microvascular lesions and ECM levels in each region, the Mann–Whitney *U* test was used for non-parametric analysis between patients with and without ADNC. Spearman's partial ICC were used to assess associations between the non-parametric analysis and the A score of Aβ deposits, the B score of neurofibrillary tangles, and the C score of neuritic plaques. For in vitro experiments, data are presented as mean ± SEM and analyzed using the Mann–Whitney *U* test or two-way ANOVA, followed by Bonferroni's multiple comparisons test. The significance level was set at 0.05, and all tests were two-tailed.

3 | RESULTS

A total of 12 patients were pathologically diagnosed with ADNC (AD group) and compared with 15 controls (non-AD group), which were age- and sex-matched to the AD group (Table 1). Patients in the AD group were significantly more clinically demented compared to those in the non-AD group.

3.1 | Arteriolosclerosis and venular collagenosis are more severe in AD brains

The severity of arteriolosclerosis and venular collagenosis in the white matter, cortical gray matter, putamen, and hippocampus was calculated and compared between the AD and non-AD groups (Figure 1). The distribution of microvascular pathologies varied in different brain regions. Compared to non-AD cases, arteriolosclerosis was more severe in the AD group (white matter: 0.61 vs 0.47; cortex: 0.60 vs 0.29; putamen: 0.63 vs 0.42; hippocampus: 0.45 vs 0.08), though statistical significance was found only in the putamen ($p = 0.0400$). Venular collagenosis was significantly more severe in the AD group in all four regions (white matter: 0.63 vs 0.39, $p = 0.0230$; cortex: 0.49 vs 0.22, $p = 0.0132$; putamen: 0.59 vs 0.00, $p = 0.0033$; hippocampus: 0.47 vs 0.00, $p = 0.0062$).

Associations between ABC score and microvasculature pathologies were further tested in all four brain regions (Table 2). Arteriolosclerosis severity was significantly correlated between cortical gray matter and putamen A scores, hippocampus B scores, and white matter C scores. Venular collagenosis severity was significantly associated with A, B, and C scores in all four brain regions.

3.2 | ECM remolding is highly pronounced in AD brains

Levels of BM-related ECM components, including Col IV, laminin, fibronectin, perlecan, and agrin, were quantified and compared between AD and non-AD patients (Figure 2). Col IV and fibronectin levels in AD patients were significantly decreased compared to those in non-AD patients (Col IV: 1.71 vs 2.11, $p = 0.0025$; fibronectin: 3.77 vs 4.47, $p = 0.0038$), while no difference in the laminin level was observed (2.82 vs 2.68, $p = 0.5171$). For HSPG, agrin levels in the AD group were significantly increased compared to those in the non-AD group (1.79 vs 1.35, $p < .0001$); perlecan levels in both groups were extremely low, and no significant difference was observed between the two groups (0.59 vs 0.60, $p = 0.4639$).

3.3 | Elevated agrin is associated with BBB disruption and pericytes decrease

Previous research indicated that alterations in ECM proteins can lead to disruptions in the BBB. Significant agrin deposition was detected in the microvascular system (Figure 3A); its impact might have been mainly on endothelial cells and pericytes that share the ECM with each other. PDGFRβ, a marker of pericytes, is significantly reduced in AD brains (0.69 vs 0.92, $p < .0001$, Figure 3A), suggesting a decrease in the number of pericytes. Moreover, pericytes also help regulate cerebral blood flow, leading to changes in BBB permeability. In our study, we employed immunofluorescence costaining for agrin, claudin-5, and PDGFRβ on brain slices to determine whether these proteins were colocalized (Figure 3B). The findings revealed BBB impairment in AD brains, with a marked increase in agrin expression. This suggests that agrin may play a role in pericyte-related lesions, though the exact mechanism by which it influences the BBB remains unclear.

To further explore agrin's involvement in the BBB, we developed an in vitro BBB model which cocultured hCMEC/D3 cells with human microvascular pericytes. In this experiment, agrin (10 μg/mL) was added to the coculture model for 24 h. Immunofluorescence analysis confirmed that agrin exposure led to a reduction in PDGFRβ levels (Figures 3C and 3D). Immunoblotting of total proteins in pericytes treated with agrin also showed decreased expression of PDGFRβ and claudin-5 (Figure 3E), suggesting that agrin may contribute to pericyte death and BBB disruption.

3.4 | Agrin induces ferroptosis in pericytes

3.4.1 | Agrin inhibits pericyte proliferation

To investigate the effect of agrin on pericytes, we incubated human microvascular pericytes with different concentrations of agrin (5, 10, and 50 μg/mL) for various durations (1, 2, 6, 12, and 24 h) to evaluate the impact on pericyte proliferation with a CCK-8 kit. The results showed that with increasing agrin concentration and treatment duration, the level of inhibition on human microvascular pericyte proliferation gradually increased, and after treatment with 10 and 50 μg/mL agrin for 24 h, pericyte proliferation was significantly inhibited (12 h, $p = 0.0056$; 24 h, $p = 0.0013$; Figure 4A). Therefore, we used 10 μg/mL agrin treatment for 24 h in subsequent cell experiments. The results were significant, indicating that agrin could inhibit pericyte proliferation in a time- and concentration-dependent manner.

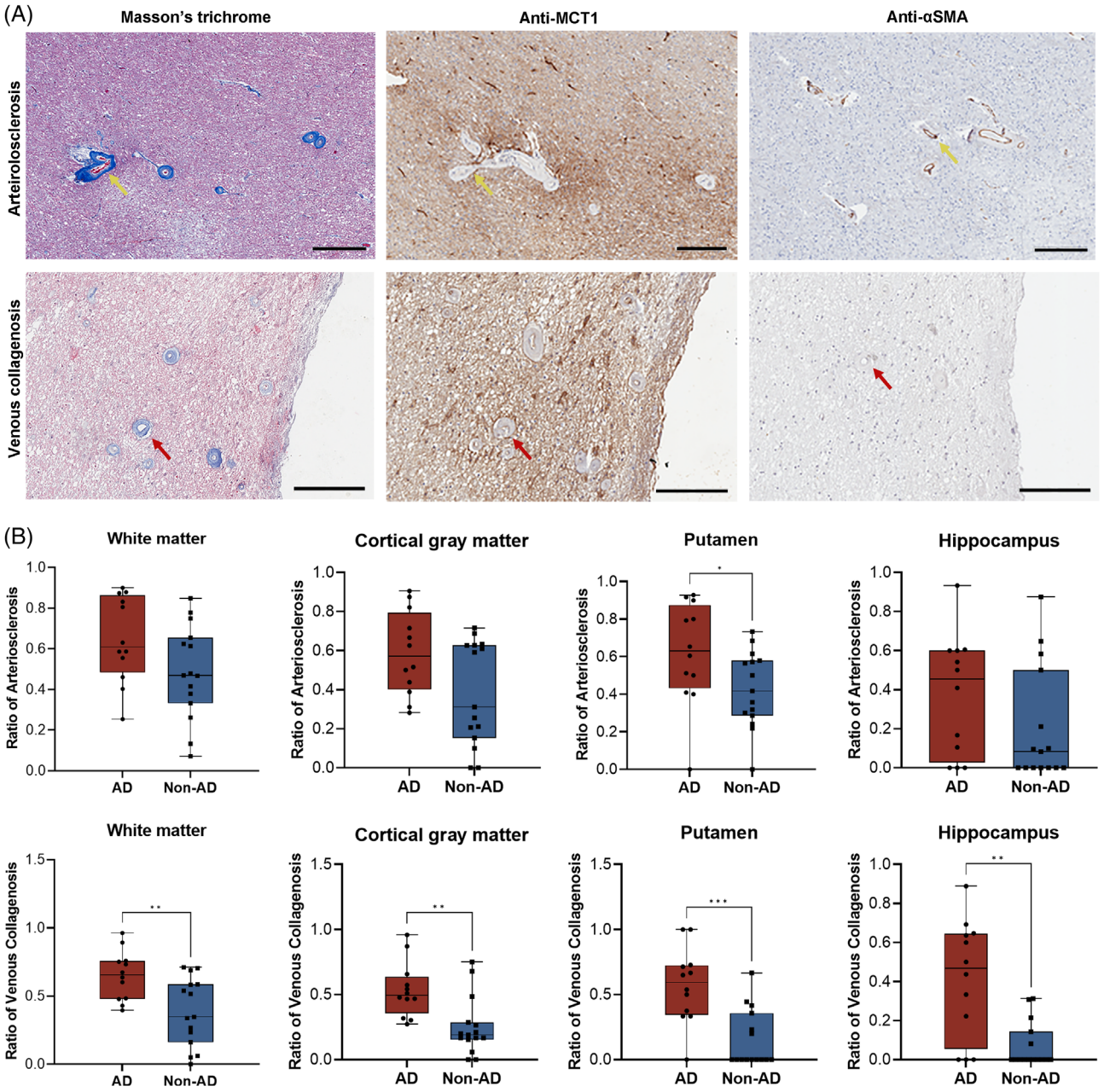

FIGURE 1 Microvasculature changes in AD and non-AD groups. (A) Features of arteriolosclerosis (yellow arrow) and venous collagenosis (red arrow) in AD and non-AD cases. Bar = 300 μm for arteriolosclerosis and 200 μm for venular collagenosis. (B) Data in each brain region are shown as median and range. Each point indicates individual ratio of immunopositivity. Statistical analysis conducted using Mann–Whitney *U* test. Ratio of arteriolosclerosis = number of sclerotic arterioles/total number of arterioles per region; ratio of venular collagenosis = number of affected venules/total number of venules per region. $^{*}p < 0.05$; $^{**}p < 0.01$; $^{***}p < 0.001$. Antibody used: αSMA (Cell Signaling Technology, 19245, 1:400), MCT1 (Proteintech, 20139-1-AP, 1:800).

3.4.2 | Agrin does not cause pericytes apoptosis but increases oxidative stress

To assess whether agrin induced pericyte apoptosis, we measured apoptotic changes using flow cytometry. Apoptosis was assessed by annexin-V/PI double staining, but no significant differences were observed (Figure 4C), suggesting agrin did not trigger apoptosis. Nevertheless, the decline in pericyte numbers and BBB disruption were evident as shown earlier. We further investigated the cause of cell death by examining oxidative stress in human microvascular pericytes using ROS fluorescent probes. The ROS kit indicated an increase in red fluorescence (639,200 vs 30,911, $p = 0.0036$, Figure 4B), which reflects elevated ROS levels in cells treated with agrin, pointing to heightened oxidative stress in pericytes.

TABLE 2 Associations between ABC score and microvascular pathology.

	White matter (β, p value)	Cortical grey matter (β, p value)	Putamen (β, p value)	Hippocampus (β, p value)
Arteriolosclerosis				
A score[a]	0.342, 0.081	0.387, 0.046*	0.410, 0.034*	0.378, 0.052
B score[b]	0.361, 0.065	0.448, 0.019*	0.345, 0.078	0.405, 0.036*
C score[c]	0.451, 0.018*	0.381, 0.050	0.350, 0.074	0.260, 0.191
Venous collagenosis				
A score	0.476, 0.012*	0.608, <0.001***	0.617, <0.001***	0.607, <0.001***
B score	0.604, <0.001***	0.598, <0.001***	0.558, 0.003**	0.600, <0.001***
C score	0.664, <0.001***	0.624, <0.001***	0.620, <0.001***	0.665, <0.001***

[a]A score, assessment of Thal phases of Aβ deposition.
[b]B score, Braak staging of neurofibrillary pathology.
[c]C score, Consortium to Establish a Registry for Alzheimer's Disease (CERAD) scoring.
*$p < .05$; **$p < .01$; ***$p < .001$.

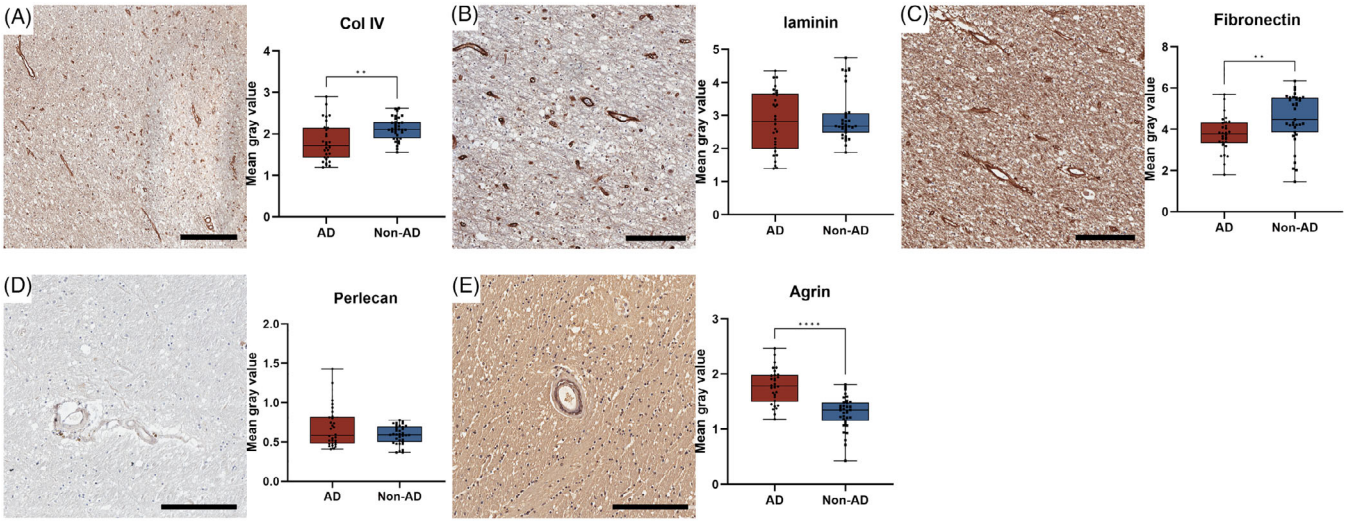

FIGURE 2 Extracellular matrix proteins in AD and non-AD groups. (A–E) Immunostaining features of collagen IV, laminin, fibronectin, perlecan, and agrin are shown in. Data of protein quantifications and comparisons between AD and non-AD groups are shown as median and range ($n = 5$). Each point indicates individual ratio of immunopositivity. Statistical analysis conducted using Mann–Whitney *U* test. Bar = 300 μm for (A) and 200 μm for (B) to (E); **$p < .01$. Antibody used: Col IV (Abcam, ab6586, 1:800), laminin (Abcam, ab11575, 1:400), fibronectin (Abcam, ab2413, 1:800), perlecan (Abcam, ab23418, 1:100), agrin (Abcam, ab85174, 1:100).

3.4.3 | Agrin induces an ROS increase in pericytes, leading to ferroptosis

Ferroptosis, a newly recognized form of cell death, occurs through the accumulation of lipid ROS in an iron-dependent process. Glutathione peroxidase 4 (GPX4), an essential enzyme for neutralizing lipid ROS, plays a critical role in preventing ferroptosis. Additionally, ferritin heavy chain 1 (FTH1) is a key iron storage protein that regulates intracellular iron homeostasis, helping to prevent excess free iron, which could otherwise catalyze the formation of ROS and promote ferroptosis. In our study, agrin stimulation of pericytes resulted in increased ROS production, leading us to hypothesize that agrin might be driving ferroptosis. To test this, we treated human microvascular pericytes with both agrin and erastin (a ferroptosis inducer). The results showed that, compared to the control group, treatment with agrin significantly increased intracellular Fe^{2+} levels, as indicated by the elevated fluorescence intensity of FerroOrange, similar to the levels observed in the erastin-treated (10 μM, 12 h) group (agrin vs CTL, $p = .0017$; erastin vs CTL, $p < 0.0001$; agrin vs erastin, $p = .4431$; Figure 4D). However, the addition of the ferroptosis inhibitor Fer-1 effectively restored Fe^{2+} levels, bringing them back to levels comparable to the control group (Agrin+Fer1 vs CTL, $p > 0.9999$). Moreover, agrin and erastin treat-

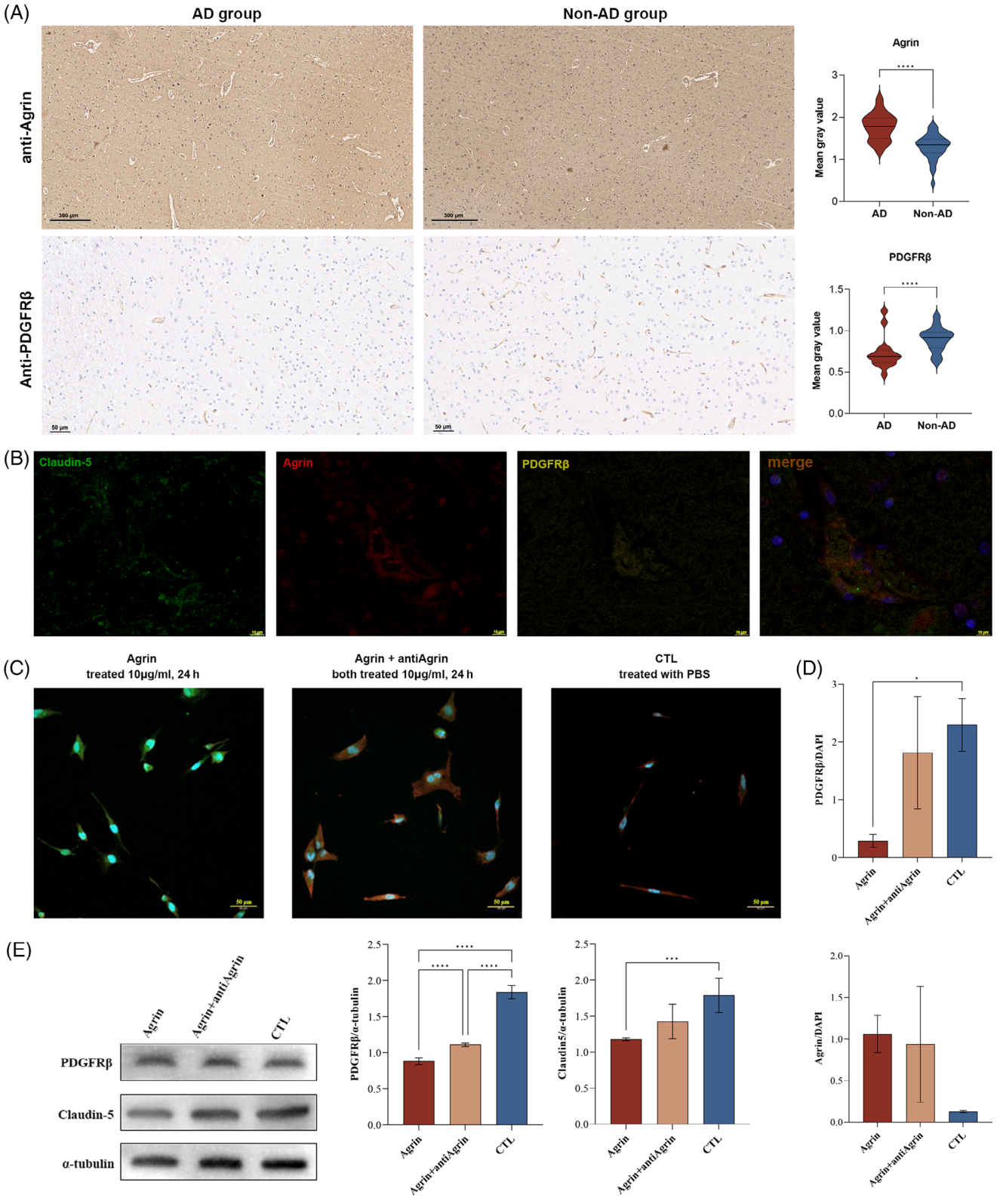

FIGURE 3 The BBB of AD brains is damaged with elevated agrin deposition and reduced pericytes. (A) Immunohistochemical staining shows that the deposition of agrin is severer (bar = 300 μm) while PDGFRβ is lower (bar = 50 μm) in the AD group. The inverted mean gray values of the area immunoreactive for DAB staining were measured from five images (1 × 1 mm) captured randomly using ImageJ software. The data are presented as median and interquartile range. Statistical analysis conducted using Mann–Whitney *U* test. Antibody used: agrin (Sigma-Aldrich, MAB5204, 1:500), PDGFRβ (Proteintech, 13449-1-AP, 1:500). (B) Immunofluorescence shows that claudin-5 (green) and agrin (red) are colocalized in pericytes (yellow), and blue indicates DAPI (bar = 10 μm). Antibody used: claudin-5 (Proteintech, 29767-1-AP, 1:500), agrin

ment led to a marked reduction in GPX4 and FTH1 protein expression levels (Figure 4E). These findings strongly indicate that agrin induces ferroptosis in pericytes.

4 | DISCUSSION

The objective of this study was to describe and quantify changes in both the microvascular medium tunica and ECM components and to compare these changes between the AD and non-AD groups. We found a higher proportion of sclerotic arterioles and collagenic venules in patients with ADNC, whereas only the severity of collagenized venules was notable. ECM protein evaluations showed that the expression of Col IV and fibronectin was lower and that of agrin was higher in AD cases that may represent microvascular dysfunction, which was independent of age. Our findings suggest that not only is the medium tunica damaged but the BM-related ECM is also affected with ADNC in the microvasculature of the brain parenchyma, and the venules are more diseased.

4.1 | Microvascular media tunica pathology

Notably, in this study, the severity of collagenized venules was more significantly correlated with ADNC, which is the most important finding concerning the potential role of venules in AD progression seldom known from previous histopathological studies. This is partly because small vessels have seldom been differentiated into arterioles or venules in previous studies. With the accumulating knowledge of the glymphatic system, there is increasing speculation that structural alterations causing venule and vein drainage might also contribute to AD pathology, while amyloid might be eliminated from the brain along the perivenous spaces in the glymphatic system.[31] In a study of amyloid precursor protein and presenilin one rat, venous collagenosis was also observed in the leptomeningeal, cortical, hippocampal, and cerebellar areas.[32] Notably, the involved veins and venules stained positive for Aβ and tau, indicating the concurrent deposition of collagen and amyloid. However, direct evidence in humans is lacking. MRI-visible deep medullary venules showed a higher tortuosity in patients with early AD in a 7T imaging study,[33] and our previous MRI data also suggested a significant correlation between fewer deep medullary venules and brain atrophy,[34] further supporting the potential role of venules in age-related neurodegenerative processes. Histopathologically, studies on venular impairment in AD brains are not as plentiful as corresponding studies on arterioles, with only Keith et al. reporting the presence of venous collagenosis in AD individuals.[35] However, most previous studies suggested that periarteriolar spaces were involved in ADNC.[36] In our study, the lack of a significant association between white matter/cortex/hippocampus arteriolosclerosis and severe ADNC might be owing to the limited sample size and paucity of extensive arteriolosclerosis. However, we found that the venules were more diseased in the brain parenchyma with ADNC. Our results highlight the importance of studying the long-neglected brain venular system to understand the roles of arterioles and venules in AD progression. Additionally, venous collagenosis may also contribute to BBB dysfunction, a hallmark of AD. Structural changes in venules, particularly collagen deposition, might compromise BBB integrity by altering endothelial cell function and ECM composition. This raises the question of how venular pathology interacts with molecular pathways like agrin-mediated ferroptosis, as discussed below.

4.2 | BM-related ECM protein remolding

Endothelial cells, key components of the BBB, are covered by BM and ECM proteins in the neurovascular unit.[37] Disruption of Aβ clearance across the BBB contributes to Aβ accumulation, linking BBB dysfunction to AD pathology. Col IV, laminin, and fibronectin, core BM-related ECM components, show variable changes in AD. Some studies report increased Col IV, while others, including ours, show decreased Col IV but increased Col I and III.[13,15,18,38] Laminin and fibronectin levels are inconsistent, while perlecan and agrin are often elevated, correlating with Aβ accumulation and BBB dysfunction.[18,39–41] These discrepancies likely result from differences in study models and disease stages.[42–44] Further research into BM-ECM dynamics in AD may support therapeutic advancements targeting the BBB.

Previous research demonstrated that alterations in ECM proteins could compromise the integrity of the BBB, but the specific involvement of agrin in this process has remained unclear. Our findings confirm a significant upregulation of agrin in AD brains, correlating with BBB dysfunction. This aligns with prior reports that highlight ECM changes as a key factor in BBB impairment. However, our data extend this understanding by suggesting that agrin's elevated expression may specifically contribute to pericyte pathology, a critical component in maintaining BBB stability. To the best of our knowledge, this represents the first proposed potential mechanism, which is of great significance for identifying therapeutic targets.

c.[45] In our study, we also found that agrin affected pericyte proliferation in a concentration-dependent way. Interestingly, while pericyte numbers decreased in agrin-treated samples, flow cytometry revealed no increase in apoptosis, indicating that agrin did not induce cell death through classical apoptotic pathways. Instead, our results implicate

(Sigma-Aldrich, MAB5204, 1:500). (C) Immunofluorescence shows that agrin (green) exposure led to a reduction in PDGFRβ (red) levels (bar = 50 µm). (D) Fluorescence semiquantitative analysis of agrin and PDGFRβ. We randomly selected three 450 × 450 µm visual fields for statistical analysis ($n = 6$) using two-way ANOVA, followed by Bonferroni's multiple comparisons test. The data are presented as the means ± SEM. (E) Semiquantitative analysis of PDGFRβ and claudin-5 protein levels. Statistical analysis conducted using two-way ANOVA, followed by Bonferroni's multiple comparisons test. Data are presented as means ± SEM. $^{*}p < 0.05$; $^{***}p < 0.001$; $^{****}p < 0.0001$.

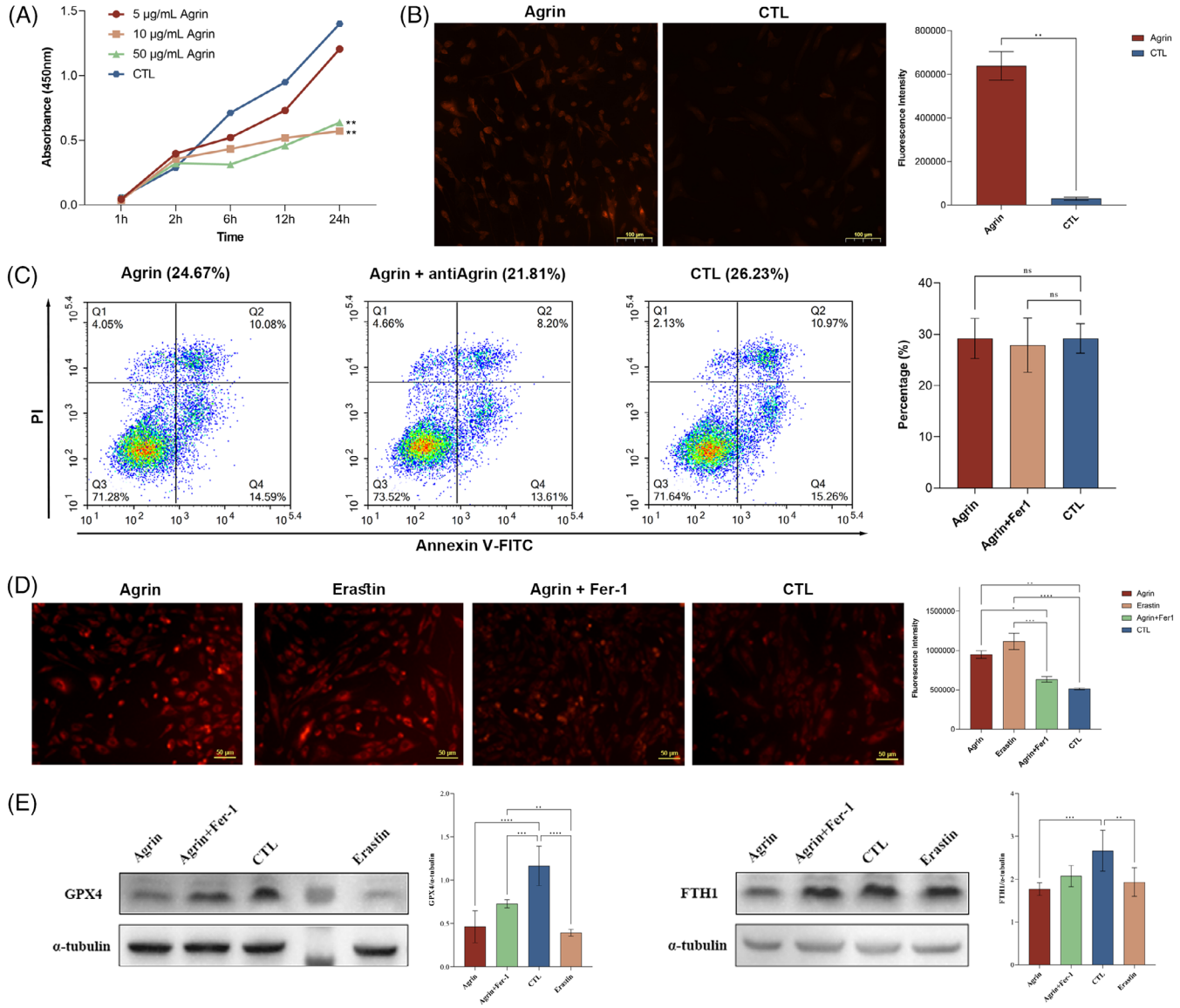

FIGURE 4 Agrin treatment of pericytes led to increased generation of ROS and ferroptosis. (A) CCK-8 assay was used to detect proliferation of pericytes after stimulation with different concentrations of agrin (5, 10, or 50 μg/mL) for various durations (1, 2, 6, 12, and 24 h) ($n = 3$). Statistical analysis conducted using two-way ANOVA. (B) Fluorescence microscopy observation and detection of fluorescent probe for ROS, which is used to show the changes in ROS expression in pericytes caused by agrin stimulation (bar = 100 μm). The data are presented as the means ± SEM ($n = 4$) and statistical analysis conducted using Mann–Whitney *U* test. (C) Flow cytometry to detect effect of agrin on pericyte apoptosis by initially staining cells with annexin V and propidium iodide (PI) solution. Cells that were PI negative and annexin V-positive cells are considered apoptotic. Data are presented as mean ± SEM ($n = 4$), and statistical analysis conducted using two-way ANOVA. (D) Representative fluorescence images of intracellular Fe^{2+} levels in four groups are shown (bar = 50 μm). Data presented as mean ± SEM ($n = 4$). Statistical analysis was performed using one-way ANOVA with post hoc testing. (E) Semiquantitative analysis of GPX4 and FTH1 protein levels. Data are presented as mean ± SEM. Statistical analysis was conducted using two-way ANOVA, followed by Bonferroni's multiple comparisons test. $^{**}p < 0.01$; $^{***}p < 0.001$; $^{****}p < 0.0001$.

ferroptosis as the underlying mechanism of pericyte death. The elevated levels of ROS and reduced expression of GPX4 and FTH1 in pericytes treated with agrin provide compelling evidence that ferroptosis, an iron-dependent form of necrosis driven by lipid peroxidation, is at play. This is further supported by the parallel effects observed with erastin, a known ferroptosis inducer, reinforcing the hypothesis that agrin accelerates oxidative stress and lipid ROS accumulation in pericytes, leading to their demise.

These findings contribute to the growing body of evidence that ferroptosis plays a critical role in neurodegenerative diseases like AD, particularly through its impact on cerebrovascular health. By inducing ferroptosis in pericytes, agrin not only promotes BBB breakdown but also exacerbates neuroinflammation and neurodegeneration. Understanding this pathway opens new therapeutic avenues, where targeting ferroptosis could help preserve pericyte function and BBB integrity, potentially slowing the progression of AD-related vascular damage.

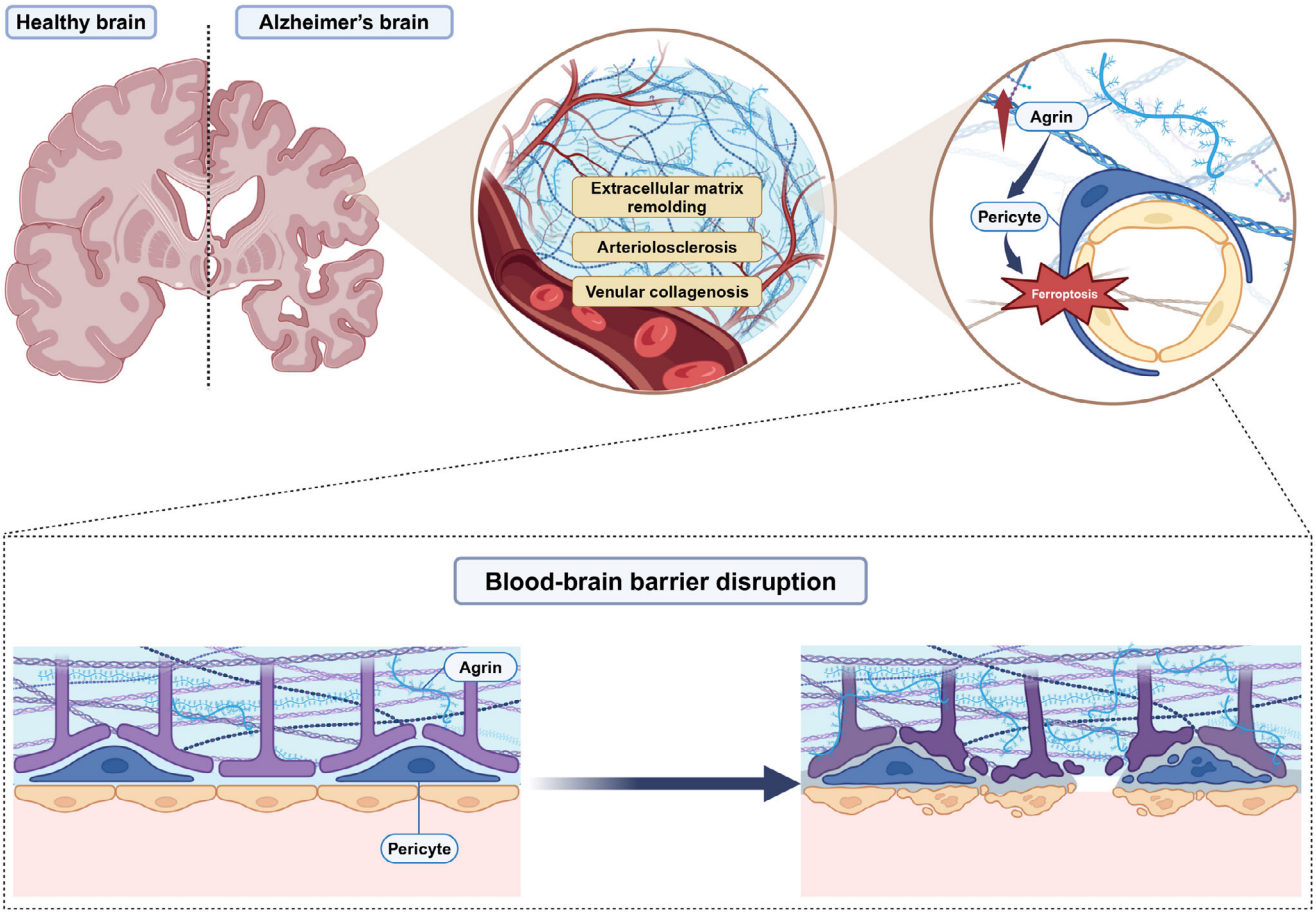

FIGURE 5 Graphical abstract summarizing results. Image was created using Adobe Photoshop 2023 with BioRender elements (https://www.biorender.com/).

Further studies are needed to delineate the precise molecular interactions between agrin, pericytes, and the ferroptosis pathway, as well as to explore the therapeutic potential of ferroptosis inhibitors in AD and related diseases.

4.3 | Integrating venous collagenosis, BBB dysfunction, and agrin-induced ferroptosis

Our findings propose a model where venous collagenosis, BBB dysfunction, and agrin-mediated ferroptosis interact to drive AD pathology. Venous collagenosis may act as an upstream factor disrupting glymphatic clearance and initiating vascular stress. Concurrently, ECM protein alterations, including agrin upregulation, exacerbate pericyte loss and BBB breakdown via ferroptosis. This vascular dysfunction likely creates a pro-inflammatory environment, facilitating amyloid accumulation and neurodegeneration.

Future studies should explore the temporal and spatial relationships between venous collagenosis, ECM protein alterations, and ferroptosis pathways in different stages of AD. A better understanding of these mechanisms could facilitate the development of therapies that address both vascular and neurodegenerative components of AD.

To the best of our knowledge, this is the first human pathological study to systematically investigate the relationship between different cerebral microvascular types and ADNC. However, this study has some limitations. The main limitation of our study is the small size of the cohort owing to the difficulty in acquiring brain tissues. Second, as in common pathological studies, the selected samples in our observational study cannot represent the whole-brain status, and we cannot rule out a casual observation. Third, limited demographic and clinical (e.g., vascular risk factors) data were available, and our findings cannot be adjusted for other underlying factors, except for age and sex. For ECM analysis, the ratio of immunopositivity to vessel areas is better than that to the selected region area. Because the microvascular area in each region is unavailable in our data, the calculated ECM changes may be partly due to changes in vessel numbers. Another point that should be noted is that the *post mortem* delay in controls is clearly, though not significantly, higher, which could reveal some possible selection bias. Our study does not include additional data to directly elucidate the mechanisms underlying the concentration-dependent effect of agrin; therefore, further investigation into the precise signaling pathways is warranted. Lastly, another limitation of this study is the inability to directly assess ferroptosis in cerebral vessels of AD brains due to the use of paraffin-embedded tissues,

which are incompatible with live-cell-based assays. Future studies utilizing frozen tissues and advanced proteomic techniques are needed to explore ferroptosis-related mechanisms in greater detail.

In summary, the results of our study further support those changes in the microvasculature, including arteriolosclerosis, venular collagenosis, and ECM remodeling, are evident in AD cases. Agrin exposure leads to ferroptosis in pericytes, ultimately compromising BBB integrity (Figure 5). Although our study is merely descriptive, our findings highlight the pathological changes in venules as a potential contributor to ADNC. As these were seldom investigated and are probably significantly different from arteriolar systems in terms of risk factors, etiology, and pathogenesis, further studies on the venular system might provide a new perspective in understanding the contribution of vascular factors to ADNC progression. Additionally, agrin-induced ferroptosis in pericytes is a potential mechanism underlying BBB disruption in AD, presenting agrin as a promising target for future therapeutic strategies aimed at preserving microvascular function and BBB integrity in AD.

ACKNOWLEDGMENTS

We thank all participants of the National Human Brain Bank for Development and Function. This work was supported by the STI2030-Major Project (2021ZD0201100) Task 5 (2021ZD0201105), the National Natural Science Foundation of China (81971138, 82301501), the Chinese Academy of Medical Sciences Innovation Fund for Medical Sciences (CIFMS 2021-I2M-1-025), and the Strategic Priority Research Program "Biological basis of aging and therapeutic strategies" of the Chinese Academy of Sciences (XDB39040300).

CONFLICT OF INTEREST STATEMENT

The authors declare no conflicts of interest. Author disclosures are available in the supporting information.

CONSENT STATEMENT

This study was approved by the guidelines of the Institutional Review Board of the Institute of Basic Medical Sciences of the Chinese Academy of Medical Sciences/Peking Union Medical College, Beijing, China (Approval Number: 009-2014, 031-2017 and 2022125). Written informed consent was obtained from both the brain donors and their next of kin.

ORCID

Yuan Cao https://orcid.org/0000-0003-4257-6908

REFERENCES

1. Jack CR Jr, Bennett DA, Blennow K, et al. NIA-AA research framework: toward a biological definition of Alzheimer's disease. *Alzheimers Dement*. 2018;14(4):535-562. doi:10.1016/j.jalz.2018.02.018
2. White LR, Edland SD, Hemmy LS, et al. Neuropathologic comorbidity and cognitive impairment in the Nun and Honolulu-Asia Aging Studies. *Neurology*. 2016;86(11):1000-1008. doi:10.1212/wnl.0000000000002480
3. Toledo JB, Arnold SE, Raible K, et al. Contribution of cerebrovascular disease in autopsy confirmed neurodegenerative disease cases in the National Alzheimer's Coordinating Centre. *Brain*. 2013;136(Pt 9):2697-2706. doi:10.1093/brain/awt188
4. Attems J, Jellinger KA. The overlap between vascular disease and Alzheimer's disease-lessons from pathology. *BMC Med*. 2014;12:206. doi:10.1186/s12916-014-0206-2
5. Esiri MM, Nagy Z, Smith MZ, Barnetson L, Smith AD. Cerebrovascular disease and threshold for dementia in the early stages of Alzheimer's disease. *Lancet*. 1999;354(9182):919-920. doi:10.1016/s0140-6736(99)02355-7
6. Mawuenyega KG, Sigurdson W, Ovod V, et al. Decreased clearance of CNS beta-amyloid in Alzheimer's disease. *Science*. 2010;330(6012):1774. doi:10.1126/science.1197623
7. Zhou M, Mao L, Wang Y, et al. Morphologic changes of cerebral veins in hypertensive rats: venous collagenosis is associated with hypertension. *J Stroke Cerebrovasc Dis*. 2015;24(3):530-536. doi:10.1016/j.jstrokecerebrovasdis.2014.09.038
8. Lin J, Lan L, Wang D, Qiu B, Fan Y. Cerebral Venous collagen remodeling in a modified white matter lesions animal model. *Neuroscience*. 2017;367:72-84. doi:10.1016/j.neuroscience.2017.10.031
9. Cassot F, Lauwers F, Lorthois S, Puwanarajah P, Cances-Lauwers V, Duvernoy H. Branching patterns for arterioles and venules of the human cerebral cortex. *Brain Res*. 2010;1313:62-78. doi:10.1016/j.brainres.2009.12.007
10. Lorthois S, Lauwers F, Cassot F. Tortuosity and other vessel attributes for arterioles and venules of the human cerebral cortex. *Microvasc Res*. 2014;91:99-109. doi:10.1016/j.mvr.2013.11.003
11. Brown WR, Thore CR. Review: cerebral microvascular pathology in ageing and neurodegeneration. *Neuropathol Appl Neurobiol*. 2011;37(1):56-74. doi:10.1111/j.1365-2990.2010.01139.x
12. Sun Y, Xu S, Jiang M, et al. Role of the extracellular matrix in Alzheimer's disease. *Front Aging Neurosci*. 2021;13:707466. doi:10.3389/fnagi.2021.707466
13. Damodarasamy M, Vernon RB, Pathan JL, et al. The microvascular extracellular matrix in brains with Alzheimer's disease neuropathologic change (ADNC) and cerebral amyloid angiopathy (CAA). *Fluids Barriers CNS*. 2020;17(1):60. doi:10.1186/s12987-020-00219-y
14. Reed MJ, Damodarasamy M, Banks WA. The extracellular matrix of the blood-brain barrier: structural and functional roles in health, aging, and Alzheimer's disease. *Tissue Barriers*. 2019;7(4):1651157. doi:10.1080/21688370.2019.1651157
15. Christov A, Ottman J, Hamdheydari L, Grammas P. Structural changes in Alzheimer's disease brain microvessels. *Curr Alzheimer Res*. 2008;5(4):392-395. doi:10.2174/156720508785132334
16. Hawkes CA, Gatherer M, Sharp MM, et al. Regional differences in the morphological and functional effects of aging on cerebral basement membranes and perivascular drainage of amyloid-β from the mouse brain. *Aging Cell*. 2013;12(2):224-236. doi:10.1111/acel.12045
17. Hawkes CA, Härtig W, Kacza J, et al. Perivascular drainage of solutes is impaired in the ageing mouse brain and in the presence of cerebral amyloid angiopathy. *Acta Neuropathol*. 2011;121(4):431-443. doi:10.1007/s00401-011-0801-7
18. Lepelletier FX, Mann DM, Robinson AC, Pinteaux E, Boutin H. Early changes in extracellular matrix in Alzheimer's disease. *Neuropathol Appl Neurobiol*. 2017;43(2):167-182. doi:10.1111/nan.12295
19. Scioli MG, Bielli A, Arcuri G, Ferlosio A, Orlandi A. Ageing and microvasculature. *Vascular Cell*. 2014;6:19. doi:10.1186/2045-824x-6-19
20. Wolburg H, Noell S, Wolburg-Buchholz K, Mack A, Fallier-Becker P. Agrin, aquaporin-4, and astrocyte polarity as an important feature of the blood-brain barrier. *Neuroscientist*. 2009;15(2):180-193. doi:10.1177/1073858408329509
21. Li J, Li M, Ge Y, et al. β-amyloid protein induces mitophagy-dependent ferroptosis through the CD36/PINK/PARKIN pathway leading to blood-brain barrier destruction in Alzheimer's disease. *Cell Biosci*. 2022;12(1):69. doi:10.1186/s13578-022-00807-5

22. Qiu W, Zhang H, Bao A, et al. Standardized operational protocol for human brain banking in China. *Neurosci Bull*. 2019;35(2):270-276. doi:10.1007/s12264-018-0306-7
23. Montine TJ, Phelps CH, Beach TG, et al. National Institute on Aging-Alzheimer's Association guidelines for the neuropathologic assessment of Alzheimer's disease: a practical approach. *Acta Neuropathol*. 2012;123(1):1-11. doi:10.1007/s00401-011-0910-3
24. Thal DR, Rüb U, Orantes M, Braak H. Phases of A beta-deposition in the human brain and its relevance for the development of AD. *Neurology*. 2002;58(12):1791-1800. doi:10.1212/wnl.58.12.1791
25. Braak H, Alafuzoff I, Arzberger T, Kretzschmar H, Del Tredici K. Staging of Alzheimer disease-associated neurofibrillary pathology using paraffin sections and immunocytochemistry. *Acta Neuropathol*. 2006;112(4):389-404. doi:10.1007/s00401-006-0127-z
26. Mirra SS, Heyman A, McKeel D, et al. The Consortium to Establish a Registry for Alzheimer's Disease (CERAD). Part II. Standardization of the neuropathologic assessment of Alzheimer's disease. *Neurology*. 1991;41(4):479-486. doi:10.1212/wnl.41.4.479
27. Cao Y, Ao DH, Ma C, Qiu WY, Zhu YC. Immunoreactivity and a new staining method of monocarboxylate transporter 1 located in endothelial cells of cerebral vessels of human brain in distinguishing cerebral venules from arterioles. *Eur J Histochem*. 2021;65(s1). doi:10.4081/ejh.2021.3306
28. Deramecourt V, Slade JY, Oakley AE, et al. Staging and natural history of cerebrovascular pathology in dementia. *Neurology*. 2012;78(14):1043-1050. doi:10.1212/WNL.0b013e31824e8e7f
29. Skrobot OA, Attems J, Esiri M, et al. Vascular cognitive impairment neuropathology guidelines (VCING): the contribution of cerebrovascular pathology to cognitive impairment. *Brain*. 2016;139(11):2957-2969. doi:10.1093/brain/aww214
30. Moody DM, Brown WR, Challa VR, Anderson RL. Periventricular venous collagenosis: association with leukoaraiosis. *Radiology*. 1995;194(2):469-476. doi:10.1148/radiology.194.2.7824728
31. Abbott NJ, Pizzo ME, Preston JE, Janigro D, Thorne RG. The role of brain barriers in fluid movement in the CNS: is there a 'glymphatic' system?. *Acta Neuropathol*. 2018;135(3):387-407. doi:10.1007/s00401-018-1812-4
32. Klakotskaia D, Agca C, Richardson RA, Stopa EG, Schachtman TR, Agca Y. Memory deficiency, cerebral amyloid angiopathy, and amyloid-β plaques in APP+PS1 double transgenic rat model of Alzheimer's disease. *PLoS One*. 2018;13(4):e0195469. doi:10.1371/journal.pone.0195469
33. Bouvy WH, Kuijf HJ, Zwanenburg JJ, et al. Abnormalities of cerebral deep medullary veins on 7 Tesla MRI in amnestic mild cognitive impairment and early Alzheimer's disease: a pilot study. *J Alzheimers Dis*. 2017;57(3):705-710. doi:10.3233/jad-160952
34. Ao DH, Zhang DD, Zhai FF, et al. Brain deep medullary veins on 3-T MRI in a population-based cohort. *J Cereb Blood Flow Metab*. 2021;41(3):561-568. doi:10.1177/0271678X20918467
35. Keith J, Gao FQ, Noor R, et al. Collagenosis of the deep medullary veins: an underrecognized pathologic correlate of white matter hyperintensities and periventricular infarction?. *J Neuropathol Exp Neurol*. 2017;76(4):299-312. doi:10.1093/jnen/nlx009
36. Wardlaw JM, Benveniste H, Nedergaard M, et al. Perivascular spaces in the brain: anatomy, physiology and pathology. *Nat Rev Neurol*. 2020;16(3):137-153. doi:10.1038/s41582-020-0312-z
37. Yamazaki Y, Kanekiyo T. Blood-brain barrier dysfunction and the pathogenesis of Alzheimer's disease. *Int J Mol Sci*. 2017;18(9). doi:10.3390/ijms18091965
38. Kalaria RN, Pax AB. Increased collagen content of cerebral microvessels in Alzheimer's disease. *Brain Res*. 1995;705(1-2):349-352. doi:10.1016/0006-8993(95)01250-8
39. Maresh GA, Erezyilmaz D, Murry CE, Nochlin D, Snow AD. Detection and quantitation of perlecan mRNA levels in Alzheimer's disease and normal aged hippocampus by competitive reverse transcription-polymerase chain reaction. *J Neurochem*. 1996;67(3):1132-1144. doi:10.1046/j.1471-4159.1996.67031132.x
40. Osterholm C, Folkersen L, Lengquist M, et al. Increased expression of heparanase in symptomatic carotid atherosclerosis. *Atherosclerosis*. 2013;226(1):67-73. doi:10.1016/j.atherosclerosis.2012.09.030
41. Costell M, Gustafsson E, Aszódi A, et al. Perlecan maintains the integrity of cartilage and some basement membranes. *J Cell Biol*. 1999;147(5):1109-1122. doi:10.1083/jcb.147.5.1109
42. Berzin TM, Zipser BD, Rafii MS, et al. Agrin and microvascular damage in Alzheimer's disease. *Neurobiol Aging*. 2000;21(2):349-355. doi:10.1016/s0197-4580(00)00121-4
43. Donahue JE, Berzin TM, Rafii MS, et al. Agrin in Alzheimer's disease: altered solubility and abnormal distribution within microvasculature and brain parenchyma. *Proc Nat Acad Sci USA*. 1999;96(11):6468-6472. doi:10.1073/pnas.96.11.6468
44. Rauch SM, Huen K, Miller MC, et al. Changes in brain β-amyloid deposition and aquaporin 4 levels in response to altered agrin expression in mice. *J Neuropathol Exp Neurol*. 2011;70(12):1124-1137. doi:10.1097/NEN.0b013e31823b0b12
45. Gros K, Matkovič U, Parato G, et al. Neuronal agrin promotes proliferation of primary human myoblasts in an age-dependent manner. *Int J Mol Sci*. 2022;23(19):11784.doi:10.3390/ijms231911784

SUPPORTING INFORMATION

Additional supporting information can be found online in the Supporting Information section at the end of this article.

How to cite this article: Cao Y, Huang M-Y, Mao C-H, et al. Structural changes in cerebral microvasculature induced by ferroptosis contribute to blood–brain barrier disruption in Alzheimer's disease: an autopsy study. *Alzheimer's Dement*. 2025;21:e70103. https://doi.org/10.1002/alz.70103